



A 16 hr Transit of Kepler-167 e Observed by the Ground-based Unistellar Telescope Network

Amaury Perrocheau^{1,2} , Thomas M. Esposito^{1,2,3} , Paul A. Dalba^{1,4,11} , Franck Marchis^{1,2} , Arin M. Avsar⁵ , Ero Carrera⁶, Michel Douezy⁶, Keiichi Fukui⁶ , Ryan Gamurot⁶ , Tateki Goto⁶ , Bruno Guillet⁶ , Petri Kuossari⁶, Jean-Marie Laugier⁶ , Pablo Lewin^{7,8} , Margaret A. Loose⁶ , Laurent Manganese⁶, Benjamin Mirwald⁶ , Hubert Mountz⁶, Marti Mountz⁶, Cory Ostrem⁶, Bruce Parker⁶ , Patrick Picard⁶, Michael Primm⁶ , Justus Randolph⁶ , Jay Runge⁶ , Robert Savonnet⁶, Chelsea E. Sharon^{6,9} , Jenny Shih⁶ , Masao Shimizu⁶ , George Silvis⁸, Georges Simard⁶ , Alan Simpson⁶, Thusheeta Sivayogan⁶, Meyer Stein⁶, Denis Trudel⁶, Hiroaki Tsuchiyama⁶, Kevin Wagner^{6,10,12} , and Stefan Will⁶

¹ SETI Institute, Carl Sagan Center, 339 Bernardo Ave., Suite 200, Mountain View, CA 94043, USA

² Unistellar, 5 allée Marcel Leclerc, bâtiment B, Marseille, F-13008, France

³ Astronomy Department, University of California, Berkeley, CA 94720, USA

⁴ Department of Astronomy and Astrophysics, University of California, Santa Cruz, CA 95064, USA

⁵ Lunar and Planetary Laboratory, University of Arizona, Tucson, AZ 85721, USA

⁶ Unistellar Citizen Scientist

⁷ The Maury Lewin Astronomical Observatory, Glendora, CA, USA

⁸ Exoplanet Watch Citizen Scientist

⁹ Yale-NUS College, 16 College Ave West 01-220, 138527, Singapore

¹⁰ Department of Astronomy and Steward Observatory, University of Arizona, 933 N Cherry Ave., Tucson, AZ 85721, USA

Received 2022 September 5; revised 2022 October 31; accepted 2022 November 1; published 2022 November 28

Abstract

More than 5000 exoplanets have been confirmed and among them almost 4000 were discovered by the transit method. However, few transiting exoplanets have an orbital period greater than 100 days. Here we report a transit detection of Kepler-167 e, a “Jupiter analog” exoplanet orbiting a K4 star with a period of 1071 days, using the Unistellar ground-based telescope network. From 2021 November 18 to 20, citizen astronomers located in nine different countries gathered 43 observations, covering the 16 hr long transit. Using a nested sampling approach to combine and fit the observations, we detected the midtransit time to be UTC 2021 November 19 17:20:51 with a 1σ uncertainty of 9.8 minutes, making it the longest-period planet to ever have its transit detected from the ground. This is the fourth transit detection of Kepler-167 e, but the first made from the ground. This timing measurement refines the orbit and keeps the ephemeris up to date without requiring space telescopes. Observations like this demonstrate the capabilities of coordinated networks of small telescopes to identify and characterize planets with long orbital periods.

Unified Astronomy Thesaurus concepts: [Exoplanets \(498\)](#); [Transits \(1711\)](#); [Amateur astronomers \(34\)](#); [Exoplanet detection methods \(489\)](#); [Transit photometry \(1709\)](#); [Astronomy data analysis \(1858\)](#); [Observatories \(1147\)](#); [Light curves \(918\)](#); [Optical telescopes \(1174\)](#); [Observational astronomy \(1145\)](#); [Astronomy education \(2165\)](#); [Astronomy data modeling \(1859\)](#)

1. Introduction

Around 800 exoplanets are known to have an orbital period of more than 100 days, based on data extracted from the NASA Exoplanet Archive¹³ (NEA; Akeson et al. 2013; NASA Exoplanet Archive 2022). Out of these 800, only ~ 170 have been detected using the transit method. This is primarily because the probability of observing an exoplanet transit decreases as the planet’s orbital semimajor axis increases, but also because the relatively small fraction of its orbit that a planet spends in transit requires almost continuous observation for detection (Beatty & Gaudi 2008). While the probability of detection does increase with orbital eccentricity, with periastron becoming smaller, the time between transits remains long (e.g., Kane 2007;

Dalba et al. 2021). Freed from the constraints of ground-based observations, the Kepler (Borucki et al. 2010) and Transiting Exoplanet Survey Satellite (TESS; Ricker et al. 2014) missions enabled great progress in the search for long-period exoplanets by providing long continuous baseline transit surveys (Wang et al. 2015; Uehara et al. 2016; Herman et al. 2019), although for TESS this is true only near the ecliptic poles.

Studying these long-period planets is crucial to understanding our own solar system. Jupiter has an orbital period of 12 yr but dominates the planets’ gravitational effects and is partly responsible for the current architecture of the solar system due to its migrations (e.g., Tsiganis et al. 2005; Walsh et al. 2011). It is possible to observe some of these long-period exoplanets transiting only once every few years and it requires substantial observation time on space telescopes to detect those with periods that are unknown or poorly constrained (Foreman-Mackey et al. 2016). Observing them from the ground is even harder because of the Sun’s daily interference and the long durations of these transits; of the confirmed planets with period >100 days and a measured duration, all but one have a duration >3.5 hr (NEA), meaning at least a 7 hr observation is required to gather equal amounts of in-transit and out-of-transit data.

¹¹ Heising-Simons 51 Pegasi b Postdoctoral Fellow.

¹² NASA Hubble Fellowship Program—Sagan Fellow.

¹³ As of 2022 September 2.



From the ground, therefore, only a network of telescopes spanning the globe is capable of capturing enough of the transit to lead to a detection (Von Braun et al. 2009). The longest-period transiting planet previously detected was HIP 41378 f (542 days) and it required four professional telescopes in Chile, Spain, and Italy, only two of which actually captured a combined ~ 3 hr of in-transit data out of the 19 hr event (Bryant et al. 2021). Similarly, two observing sites in Spain (Garcia-Melendo & McCullough 2009) and the United Kingdom (Fossey et al. 2009) detected only egress of the first observed 12 hr long transit by HD 80606 b (111 day period); admirable considering the midtransit date was only predicted within a ~ 1 day window (Laughlin et al. 2009). Redetection of a nearly complete transit by HD 80606 b by Pearson et al. (2022) via global coordination of ground-based telescopes, including Unistellar Network eVscopes, illustrates the value of geographically distributed observations.

Here, we present the first ground-based detection of the transiting “Jupiter analog” Kepler-167 e with observations by the Unistellar Network (Marchis et al. 2019). Kepler-167 e has a period of $1071.23205^{+0.00059}_{-0.00058}$ days (Chachan et al. 2022) and transit duration of 16.25 ± 0.07 hr (taken as the mean duration of 16,000 sample models drawn from the Chachan et al. 2022 posterior distribution). With a radius between that of Jupiter and Saturn ($0.9 R_J$), it has about the same mass as Jupiter ($1.01 M_J$) and a low orbital eccentricity (0.06; Kipping et al. 2016). It orbits a K4V star with $V = 14.284$, along with three inner super-Earth planets that also transit (Kipping et al. 2016). The Kepler mission enabled the first two observations, in 2010 and in 2013 (Kipping et al. 2016), and half a transit was observed in 2018 with the Spitzer Space Telescope (Werner et al. 2004) to rule out transit timing variations (TTV) of at least 34 minutes to 3σ confidence (Dalba & Tamburo 2019). Thanks to these works, the uncertainty on the midtransit time (T_0) of the 2021 transit prediction was just $\sigma_{T_0} = 3.0$ min.

The Unistellar Network is composed of $\sim 10,000$ digital telescopes called Enhanced Vision Telescopes, or “eVscopes” (Marchis et al. 2020). Citizen astronomers in possession of an eVscope can be found all over the world. These telescopes have already been used to observe exoplanet transits (e.g., HD 80606 b by Pearson et al. 2022, WASP-148 b by Wang et al. 2022, TOI-2180 b by Dalba et al. 2022), time asteroid occultations (Cazeneuve et al. 2022), and monitor the James Webb Space Telescope (JWST; Lambert et al. 2022).

We describe here our observations and analyses that led to the detection of the Kepler-167 e transit. In Section 2, we present the photometric data gathered from the Unistellar Network. Section 3 describes the methods for combining the observations and modeling the transit. Section 4 presents the results and finalized light curve. Finally, Section 5 discusses the validity of our results and relevance of a ground-based telescope network for observing long-duration exoplanet transits.

2. Observations

2.1. Unistellar eVscopes

The eVscopes are portable digital consumer telescopes manufactured and distributed by Unistellar. Two hardware models are currently in use: the eVscope 1 (same as the eQuinox model) and the eVscope 2. They both have an aperture of 114.3 mm and a focal length of 450 mm. Both also use off-the-shelf Sony CMOS sensors located at the prime

focus with low read noise and dark current, with a Bayer filter. The IMX224 sensor in the eVscope 1 has a field of view (FOV) of $37' \times 28'$ with a pixel scale of $1''.72$ per pixel and the IMX347 in the eVscope 2 has an FOV of $45' \times 34'$ with a pixel scale of $1''.33$ per pixel. Each eVscope is identified by a six-digit alphanumeric string that is abbreviated in this paper to the first three characters. A suffix “-B” is added when the citizen scientist observed for a second time during the campaign with the same telescope.

2.2. Observation Campaign

Dalba & Tamburo (2019) predicted T_0 of this 2021 transit to be $2459538.2189 \text{ BJD}_{\text{TDB}} \pm 0.0021$ (a 3.0 minutes uncertainty). They also ruled out TTVs greater than 34 minutes to 3σ significance. Using this information, the SETI Institute, the scientific partner of Unistellar, made a call to the Unistellar Network on 2021 November 4 to observe the upcoming transit. In response, 31 citizen astronomers and two professional astronomers from our team observed the target star between 2021 November 18 and 20 using Unistellar eVscopes, producing 43 individual data sets. The exposure time was set at 3.970 s and the gain at $0.02245 \text{ e-ADU}^{-1}$ (40 dB). Detailed information about the observations is given in Table 2. To have enough continuous dark time to record the >16 hr transit duration (temporarily ignoring the time also required to record important out-of-transit baseline data), a single observing site would need an extreme latitude of $>76^\circ \text{ N}$; thus the necessity to combine observations from multiple longitudes around the world. Two citizen astronomers not affiliated with the Unistellar Network also observed Kepler-167 during this campaign, discussed in Section 5.1.

2.3. Observation Selection

The observations were made from various sites spread around Earth, leading to variable data quality. At that time, the Moon was $\sim 100\%$ illuminated and located $\sim 103^\circ$ from the target. Some data were not usable because of poor weather, poor atmospheric seeing, or suboptimal calibration of the telescope focus or collimation. Moreover, the relatively high sensor gain used to observe this $V = 14.3$ target caused an unexpectedly large nonlinear increase in the background sky brightness that saturated some observations made from light-polluted areas. To avoid these data, we excluded observations where at least one pixel in the target star’s point-spread function was saturated or the scatter in the relative flux residuals after model subtraction was $>10\%$. As a result, only 27 out of the 43 data sets were used in the analysis. The time distribution of observations can be found in Figure 1 in relation to the predicted transit times.

3. Methods

3.1. Photometry

The raw images received from the eVscopes in FITS format are first dark subtracted, plate solved using `Astrometry.net` (Lang et al. 2010), aligned, and then stacked in groups of 30 representing 119.1 s of integration time. This image stacking increases star signal-to-noise ratio (S/N) by reducing random noise and further mitigates photometric noise by averaging over the differing spectral responses of individual pixels caused by the Bayer filter (e.g., Lambert et al. 2022).

Next we performed differential aperture photometry on the stacked images using the `Photutils` Python package

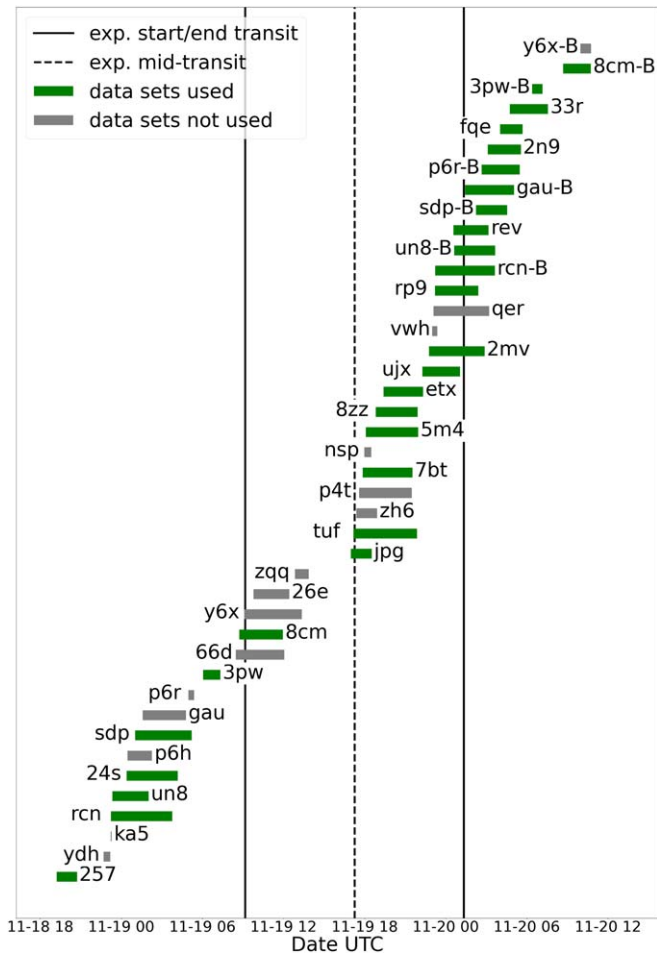


Figure 1. Time frames for eVscope observations of Kepler-167 e. 27 out of the 43 observations (green) were used to construct the final light curve. Vertical lines mark the predicted transit start, middle, and end times.

(Bradley et al. 2022). This allowed us to locate every star in an image and measure its position, flux, and uncertainty on that flux. For each data set, we identified several potential comparison stars that satisfied our criteria of being located within $3'$ of the target star, unsaturated in the individual images, and not blended with other sources. For consistency between data sets, we chose to use the same single comparison star to compute all of our relative fluxes: Gaia DR3 2051932862036924416 ($19^{\text{h}}30^{\text{m}}40^{\text{s}}.31 + 38^{\circ}19'34''14$), slightly fainter than Kepler-167 and located $1/25$ away. Being similar in magnitude to the target star meant this comparison star was also the highest S/N option that was unsaturated. We then optimized the sizes of the circular flux apertures and annular background apertures for both the target and comparison star independently by minimizing the scatter in the individual star fluxes within each data set.

3.2. Detrending

With the photometry done, we began assembling the light curve of the complete event from the individual light curves of each data set. By taking the relative flux ratio between the target and the comparison star, long-term trends in the fluxes and image-to-image photometric variations were largely removed. Trends due to differential atmospheric extinction (i.e., airmass), in particular, were greatly mitigated by the nearly identical $G_{\text{BP}} - G_{\text{RP}}$ colors of the target and comparison

stars, given by the Gaia DR3 catalog (Gaia Collaboration et al. 2016, 2022) as $(G_{\text{BP}} - G_{\text{RP}})_{\text{targ}} = 1.227932$ and $(G_{\text{BP}} - G_{\text{RP}})_{\text{comp}} = 1.190314$. No other detrending was applied. Finally, the relative fluxes of each data set are divided by their medians to normalize them to approximately 1.0 in preparation for further normalization during modeling.

We found most data sets' relative fluxes to be approximately flat over time but some did contain significant slopes. The timing of the most steeply sloped fluxes coincided with the transit's expected ingress and egress times, suggesting they were real physical features; however, we did not assume this to be the case during our analysis.

3.3. Light-curve Normalization and Modeling

Extracting the transit's signal and timing from these multiple data sets requires combining them into one light curve and comparing that with a model. Differential photometry does not establish the absolute brightness of the target star; thus, in order to properly construct a combined light curve, we need to normalize the individual light curves relative to some reference baseline. We start with the assumption that relative fluxes measured outside of the transit will have a mean of 1.0, which becomes our reference baseline.

To normalize fluxes within our model, we multiply a scalar coefficient c_i with the relative fluxes $y_{i,j}$ of every individual light curve i , where j denotes the time of each measurement. Thus, every individual light curve is free to move up and down relative to the reference baseline. We then construct a transit light-curve model using the PYCHEOPS package (Maxted et al. 2022) and fit it to the combination of all normalized fluxes. Stellar limb darkening effects are taken into account using the power-2 law as implemented in the `qpower2` algorithm (Maxted & Gill 2019).

The parameters used to compute the transit model are given in Table 1. In our approach, which aims to retrieve the transit times and depth, assuming the other transit properties are well known, we fix the following model parameters to the latest values published by Chachan et al. (2022): the planet's orbital period P , transit duration (parameterized as $P \times W$ where W is the length of the transit in orbital phase units), impact parameter b , eccentricity e (assumed to be 0), and stellar limb darkening coefficients h_1 and h_2 . As a result, only the midtransit time T_0 and the transit depth D can vary. The eccentricity measurements from Kipping et al. (2016) and Chachan et al. (2022) are both consistent with zero, so we assume the simplest case of a circular orbit. The limb darkening coefficients h_1 and h_2 are transformed parameters from the power-2 law described in Maxted et al. (2022).

3.4. Dynamic Nested Sampling

To fit our model to the data we used Bayesian statistics via a dynamic nested sampling approach (Higson et al. 2018). This method lets us estimate parameters from a highly multidimensional model. The sampling algorithm was implemented with the `dynesty` Python package (Speagle 2020), which required two functions: the prior transformation and the likelihood function.

The prior transformation converts a hypercube of values between 0 and 1 to physical scales. To avoid biasing the result toward a particular midtransit time, we used a uniform prior for T_0 . The prior bounds are chosen to be the expected $T_0 \pm$ the upper limit of the smallest TTV magnitude ruled out at 5σ

Table 1
Transit Parameters Values

Parameter	Expected Value	Distribution Priors	Best Fit
T_0 (BJD _{TDB})	2459538.2189 ± 0.0021	$\mathcal{U}[2459538.1793, 2459538.2585]$	2459538.2225 ± 0.0068
D (%)	$1.540^{+0.027}_{-0.032}$	$\mathcal{N}(1.540, 4)$	1.77 ± 0.42
$W \times P$ (minutes)	975 ± 4		
P (days)	$1071.23205^{+0.00058}_{-0.00059}$	Fixed	
b	$0.271^{+0.051}_{-0.073}$		
e	0		
h_1	0.684 ± 0.011		
h_2	0.434 ± 0.050		
c_1 (257)	1		0.997 ± 0.007
c_2 (rcn)	1		1.001 ± 0.003
c_3 (un8)	1		0.998 ± 0.006
c_4 (24s)	1		0.990 ± 0.006
c_5 (sdp)	1		0.992 ± 0.015
c_6 (3pw)	1		1.001 ± 0.007
c_7 (8cm)	0.993		0.992 ± 0.004
c_8 (jpg)	0.978		0.982 ± 0.009
c_9 (tuf)	0.978		0.978 ± 0.006
c_{10} (7bt)	0.979		0.982 ± 0.009
c_{11} (5m4)	0.979		0.987 ± 0.008
c_{12} (8zz)	0.979	$\mathcal{N}(1, 0.0004)$	0.987 ± 0.007
c_{13} (etx)	0.979		0.980 ± 0.015
c_{14} (ujx)	0.988		0.991 ± 0.005
c_{15} (2mv)	0.993		0.993 ± 0.004
c_{16} (rp9)	0.993		0.989 ± 0.005
c_{17} (rcn-B)	0.996		0.994 ± 0.004
c_{18} (un8-B)	0.996		0.998 ± 0.004
c_{19} (rev)	0.999		0.993 ± 0.008
c_{20} (sdp-B)	1		0.998 ± 0.008
c_{21} (gau-B)	1		0.998 ± 0.005
c_{22} (p6r-B)	1		0.998 ± 0.003
c_{23} (2n9)	1		0.987 ± 0.011
c_{24} (fqe)	1		0.997 ± 0.009
c_{25} (33r)	1		1.003 ± 0.006
c_{26} (3pw-B)	1		0.987 ± 0.008
c_{27} (8cm-B)	1		0.998 ± 0.004

Note. The transit duration is $W \times P$. Parameters h_1 and h_2 are stellar limb darkening coefficients within the PYCHEOPS model (Maxted et al. 2022). The normal prior on the normalization coefficients c_i has a mean of 1 and a standard deviation of 2%. The expected value of each c_i is the mean of the relative flux during the times of observation i as measured from a model built from the “expected” values for all parameters. The distribution priors are written as $\mathcal{U}[a, b]$ and $\mathcal{N}(\mu, \sigma^2)$ for the uniform and normal distributions, respectively.

significance by Dalba & Tamburo (2019), i.e., ± 57 minutes. For D and normalization coefficients c_i , we chose normal priors with the expected value as the mean and a 2% standard deviation. The values chosen are listed in Table 1. These priors were specifically chosen to be loose so the intrinsic likelihood would primarily drive the fit.

We assume that the flux measurements are independent and therefore drawn from a normal distribution. We consider this assumption to be justified because we confirmed that the time-averaged rms of the full light curve’s binned flux residuals (using the best-fit model) decreased with bin size at the rate that theory predicts for residuals dominated by uncorrelated white noise (Cubillos et al. 2017). The overall likelihood is then obtained by multiplying together the individual measurement likelihoods. Finally, because it is easier in practice to maximize the logarithm of the likelihood, we are left with an effective likelihood function of

$$\log \mathcal{L} = -\frac{1}{2} \sum_i \sum_j \frac{(c_i y_{i,j} - f_j)^2}{\sigma_{i,j}^2} \quad (1)$$

where $\sigma_{i,j}$ are the uncertainties associated with each relative flux measurement $y_{i,j}$, and f_j are the modeled light-curve fluxes at measurement time j .

We consider that the model fitting procedure has converged when $\log \mathcal{Z} < 0.1$, where \mathcal{Z} is the Bayesian model evidence.

4. Results

Using the nested sampling approach described in Section 3, we obtained the maximum likelihood (“best-fit”) light curve at the top of Figure 2, along with an estimation of the transit parameters. We measure T_0 to be UTC 2021 November 19 17:20:51 ± 9.8 minutes (2459538.2225 ± 0.0068 BJD_{TDB}) within the 68% confidence interval. This is statistically consistent with the predicted midtransit time of UTC 2021 November 19 17:15:35 ± 3.0 minutes (2459538.2189 ± 0.0021 BJD_{TDB}). The depth of the transit is measured to be $D = 1.77 \pm 0.42\%$ compared to the predicted $1.540^{+0.027}_{-0.032}\%$. The computed values for the normalization coefficients c_i are listed by data set in Table 1.

To test that our normalization of the individual light curves is not biasing our timing measurements, we also fit a transit model to a

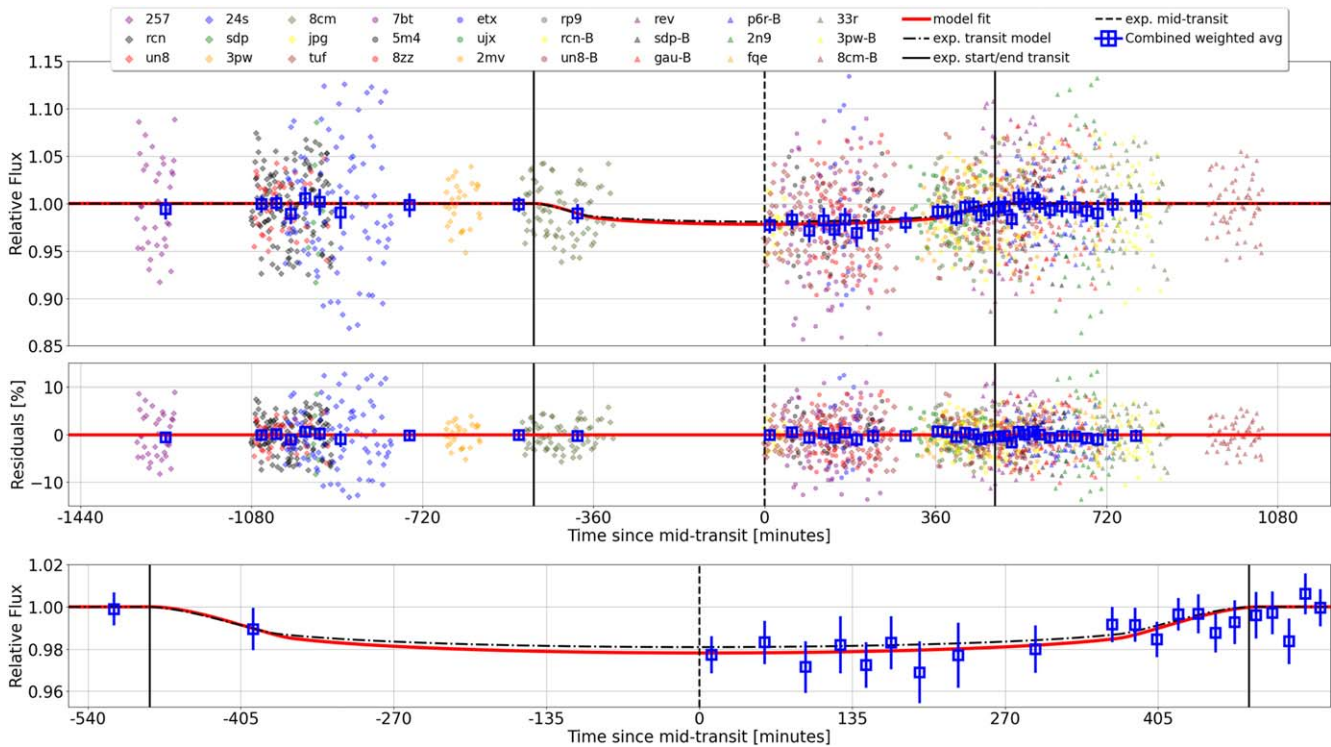


Figure 2. Transit light curve of Kepler-167 e (top) and residuals (middle) as observed by the Unistellar Network. Relative fluxes from individual data sets are plotted with different colors and symbols. The maximum likelihood model corresponding to the values in Table 1 is the red line and the time axis is defined as the time since that model’s midtransit time. The blue squares are weighted average fluxes of the combined data. The expected transit model and its transit start, middle, and end times are plotted as black broken lines. The bottom panel is the same as the top panel but zooms in on the times the transit occurred and only shows the weighted average fluxes.

light curve that excluded the fully in-transit data, which involved removing fluxes from the following data sets: *jpg*, *tuf*, *7bt*, *5m4*, *8zz*, and *etx*. This left only data sets containing at least some out-of-transit data (based on our maximum likelihood model). The resulting T_0 computed without in-transit data is UTC 2021 November 19 17:07:45 ± 11 minutes (2459538.2134 ± 0.0073 BJD_{TDB}) and the depth is 1.20% ± 0.48%. This transit depth is still consistent with the prediction and the two configurations—with and without the in-transit data—are consistent with each other at the 1 σ level.

5. Discussion

5.1. Exoplanet Watch Observation

Two citizen astronomers (Lewin and Silvis) participating in NASA’s Exoplanet Watch program (EW; Zellem et al. 2020) observed Kepler-167 during the same campaign in November 2021. We acquired their data from the public database hosted by the American Association of Variable Star Observers.¹⁴ Lewin observed a flat light curve in data taken well before the expected transit ingress, but Silvis observed during the expected egress with a 12 inch (30 cm) telescope (Table 2). Those relative fluxes, after being detrended with a standard airmass correction function, are plotted in Figure 3 and overlaid with the maximum likelihood transit model computed from our “best-fit” parameters of Table 1. The systematic “wobble” in the light curve at $X \approx 388\text{--}407$ corresponds to a temporary increase in image background level from environmental light pollution (a house light being turned on). Following this, increasing air

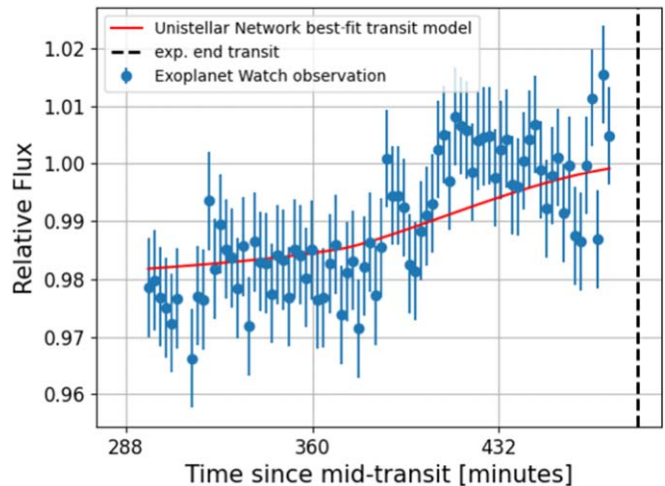


Figure 3. Exoplanet Watch observation of the Kepler-167 e egress. Relative fluxes are the blue dots, with corresponding 1 σ error bars. The best-fit transit model from fitting only Unistellar Network data is overlaid in red. This model was not fit to the Exoplanet Watch observations.

mass (from 1.4 to 1.6) and a broadening PSF may have introduced additional systematic noise via imperfect background subtraction. The last 10 flux points were strongly affected by the local horizon vignetting the entrance pupil, a systematic error not encompassed by their error bars.

Without conducting any additional fitting, the χ^2 and the reduced χ^2_ν values between our transit model and the EW fluxes are $\chi^2 = 65.9$ and $\chi^2_\nu = 0.82$, respectively. In contrast, the

¹⁴ <https://www.aavso.org/>

corresponding values when comparing the EW fluxes with a flat model normalized to the median of the detrended data are $\chi^2(\text{flat}) = 146.6$ and $\chi^2_\nu(\text{flat}) = 1.81$. We consider this an independent confirmation that the Unistellar Network data successfully detected the egress of the transit.

5.2. Observing Exoplanet Transits with a Network of Small Ground-based Telescopes

This successful measurement of Kepler-167 e proves that it is possible to detect a long-period, long-duration exoplanet transit with a network of small ground-based telescopes. Even though we knew the exoplanet parameters precisely before the transit occurred in this case, we can reproduce this result for planet candidates that have their properties less constrained. Using small telescopes such as the eVscope therefore permits the detection and confirmation of planet candidates with imprecisely known orbital periods without requiring observation time on in-demand space telescopes such as JWST or the Hubble Space Telescope (HST). A mission like ESA’s current CHAracterising ExOPlanet Satellite, which can do long-duration follow-up, could also benefit from a small-telescope network because it has its own observability limitations owing to its orbit and Earth occultations (Benz et al. 2020).

Keeping transiting planet ephemerides “fresh” (i.e the 1σ uncertainty in the midtransit time to less than half the transit duration) is crucial; for instance, most of the ephemerides coming from TESS will be outdated only 1 yr after the last observation (Dragomir et al. 2020). This concern is not limited to transiting planets, as radial velocity-detected planets also need to be monitored (Kane et al. 2009). Zellem et al. (2020) proved that uncertainties of just 1 minute in a planet’s orbital period and midtransit time will produce an uncertainty of ~ 15 hr in that planet’s midtransit time 10 yr later. Thus, regular redetections with small ground-based telescopes are important to paving the way for detailed spectroscopic characterization by JWST and subsequent generations of exoplanet characterizing facilities.

5.3. Transit Timing Consistency and Future Studies

Our timing measurement supports the previous finding by Dalba & Tamburo (2019) that Kepler-167 e’s ephemeris does not contain large TTVs. The difference between our measured midtransit epoch and the initial transit epoch recomputed by Chachan et al. (2022) is 4284.9349 ± 0.0068 days, which when divided by four equates to an orbital period of 1071.2337 ± 0.0017 days. This is in line with the Kipping et al. (2016) value of $P = 1071.23228 \pm 0.00056$ days and $P = 1071.23205^{+0.00059}_{-0.00058}$ from Chachan et al. (2022), though about 2 minutes longer than both. Using our best-fit midtransit time as a reference epoch to compute future midtransit times, we obtain values that fall within the Dalba & Tamburo (2019) 1σ predictions, but we do not improve upon their precision so we do not report new values here. The relatively large uncertainty on the previous epoch’s measurement from Spitzer data also prevents us from tightly constraining TTVs over the planet’s last orbit, but we can rule out 24 and 73 minutes TTVs to

1σ and 3σ significance, respectively. Our own measurement uncertainty will be the dominant factor in ruling out even smaller TTVs over the next orbit; thus, improved timing precision for the next transit (e.g., with greater telescope coverage from our network) will be a future objective.

The lack of large TTVs means that future observations by telescopes like HST or JWST will not run the risk of missing substantial portions of valuable in-transit time for Kepler-167 e. It is rare for such a long-period (and low-temperature) planet to be so well characterized with an unambiguous ephemeris and measured mass and radius. Therefore, we encourage additional work to explore this planet’s suitability for expanded characterization of its atmosphere and potential exomoons.

The authors thank all the citizen astronomers that participated in this observation campaign and contributed their precious data. We also thank Rob Zellem for his contributions to this research effort and the anonymous reviewer for the thoughtful feedback.

This research has made use of the NASA Exoplanet Archive, which is operated by the California Institute of Technology, under contract with the National Aeronautics and Space Administration under the Exoplanet Exploration Program. This work has also made use of data from the European Space Agency (ESA) mission Gaia (<https://www.cosmos.esa.int/gaia>), processed by the Gaia Data Processing and Analysis Consortium (DPAC, <https://www.cosmos.esa.int/web/gaia/dpac/consortium>). Funding for the DPAC has been provided by national institutions, in particular the institutions participating in the Gaia Multilateral Agreement.

This publication makes use of data products from Exoplanet Watch, a citizen science project managed by NASA’s Jet Propulsion Laboratory on behalf of NASA’s Universe of Learning. This work is supported by NASA under award number NNX16AC65A to the Space Telescope Science Institute, in partnership with Caltech/IPAC, Center for Astrophysics|Harvard & Smithsonian, and NASA Jet Propulsion Laboratory. We acknowledge with thanks the variable star observations from the AAVSO International Database contributed by observers worldwide and used in this research.

T.M.E., F.M., and the Unistellar Network’s science campaigns are supported in part by a grant from the Gordon and Betty Moore Foundation. P.D. acknowledges support from a National Science Foundation (NSF) Astronomy and Astrophysics Postdoctoral Fellowship under award AST-1903811 and a 51 Pegasi b Postdoctoral Fellowship from the Heising-Simons Foundation.

Software: Astrometry.net (Lang et al. 2010), Astropy (Astropy Collaboration et al. 2013, 2018), dynesty (Speagle 2020), Photutils (Bradley et al. 2022), PYCHEOPS (Maxted et al. 2022).












Appendix Summary of Observations













The times, locations, telescopes, and observer names for the Kepler-167 e observations analyzed in this work are given in Table 2. The time given is the length of the full observation but useful data may not have been acquired during that entire period.

Table 2
Observations Summary

eVscope ID (Abbreviated)	eVscope Model	UTC Start Date	Start Time (hh:mm:ss)	End Time ^a (hh:mm:ss)	Observer	Location
257	1	2021 Nov 18	19:13:08	20:43:19	Kuossari	Tervakoski, Finland
ydh	1	2021 Nov 18	22:41:19	23:11:10	Stein	Lakewood, NJ, USA
ka5	1	2021 Nov 18	23:12:51	23:16:53	Mountz	Louisville, KY, USA
rcn	2	2021 Nov 18	23:14:21	03:46:22	Randolph	Athens, GA, USA
un8	1	2021 Nov 18	23:20:08	02:01:20	Randolph	Athens, GA, USA
24s	1	2021 Nov 19	00:23:36	04:10:57	Ostrem	Ames, IA, USA
p6h	1	2021 Nov 19	00:27:55	02:16:24	Sivayogan	Raleigh, NC, USA
sdp	1	2021 Nov 19	01:01:20	05:12:44	Wagner	Tucson, AZ, USA
gau	1	2021 Nov 19	01:35:23	04:47:26	Loose	San Diego, CA, USA
p6r	1	2021 Nov 19	04:58:17	05:23:01	Dalba	Santa Cruz, CA, USA
3pw	1	2021 Nov 19	06:02:37	07:20:14	Gamurot	Kapolei, HI, USA
66d	1	2021 Nov 19	08:27:40	12:03:20	Tsuchiyama	Tokyo, Japan
8cm	1	2021 Nov 19	08:44:17	11:57:34	Shimizu	Sayo-cho, Hyogo, Japan
y6x	1	2021 Nov 19	09:05:34	13:21:17	Goto	Toyonaka, Osaka, Japan
26e	1	2021 Nov 19	09:47:06	12:25:55	Fukui	Tsukuba, Ibaraki, Japan
zqq	1	2021 Nov 19	12:50:32	13:52:24	Sharon	Singapore, Singapore
jpg	1	2021 Nov 19	16:58:59	18:32:02	Simpson	Thirsk, UK
tuf	1	2021 Nov 19	17:10:31	21:52:12	Laugier	Simiane Collongue, France
zh6	1	2021 Nov 19	17:22:46	18:55:27	Mirwald	Munich, Germany
p4t	1	2021 Nov 19	17:35:37	21:29:06	Carrera	Barcelona, Spain
7bt	1	2021 Nov 19	17:52:08	21:32:19	Manganesee	Cavaillon, France
nsp	1	2021 Nov 19	17:59:18	18:29:08	Douezy	Serignan, France
5m4	1	2021 Nov 19	18:05:36	21:57:31	Picard	Courthézon, France
8zz	1	2021 Nov 19	18:49:42	21:55:37	Savonnet	Trevignin, France
etx	1	2021 Nov 19	19:24:08	22:19:38	Guillet	Caen, France
ujx	1	2021 Nov 19	22:16:59	01:03:12	Simard	Mirabel, Québec, Canada
2mv	1	2021 Nov 19	22:45:55	02:52:39	Parker	High Bridge, NJ, USA
vwh	1	2021 Nov 19	22:52:53	23:22:44	Trudel	Saint-Lazare, Québec, Canada
qer	1	2021 Nov 19	23:06:02	03:12:28	Will	Raleigh, NC, USA
rp9	1	2021 Nov 19	23:12:10	02:24:10	Runge	Durham, NC, USA
rcn-B	2	2021 Nov 19	23:13:07	03:38:29	Randolph	Athens, GA, USA
un8-B	1	2021 Nov 19	23:13:50	03:38:47	Randolph	Athens, GA, USA
rev	1	2021 Nov 20	00:34:44	03:10:17	Primm	Austin, TX, USA
sdp-B	1	2021 Nov 20	01:01:12	04:32:26	Wagner	Tucson, AZ, USA
gau-B	1	2021 Nov 19	01:25:18	05:03:18	Loose	San Diego, CA, USA
p6r-B	1	2021 Nov 19	01:41:35	05:28:08	Dalba	Santa Cruz, CA, USA
2n9	1	2021 Nov 20	03:06:56	05:33:22	Esposito	Telegraph City, CA, USA
fqe	1	2021 Nov 20	04:01:11	05:41:29	Esposito	Telegraph City, CA, USA
33r	1	2021 Nov 20	04:44:09	07:34:08	Shih	Kahului, HI, USA
3pw-B	1	2021 Nov 20	04:44:38	07:09:16	Gamurot	Kapolei, HI, USA
8cm-B	1	2021 Nov 20	08:40:41	10:43:37	Shimizu	Sayo-cho, Hyogo, Japan
y6x-B	1	2021 Nov 20	08:41:44	10:44:37	Goto	Toyonaka, Osaka, Japan
...	...	2021 Nov 19	01:27:41	05:41:08	Lewin ^a	Glendora, CA, USA
...	...	2021 Nov 19	22:12:20	01:10:13	Silvis ^b	Bourne, MA, USA

Notes.^a Some end times occur on the following day.^b Citizen astronomers affiliated with Exoplanet Watch, not using eVscopes. See Section 5.1.**ORCID iDs**

Amaury Perrocheau  <https://orcid.org/0000-0003-0538-8561>
 Thomas M. Esposito  <https://orcid.org/0000-0002-0792-3719>
 Paul A. Dalba  <https://orcid.org/0000-0002-4297-5506>
 Franck Marchis  <https://orcid.org/0000-0001-7016-7277>
 Arin M. Avsar  <https://orcid.org/0000-0001-7801-7425>
 Keiichi Fukui  <https://orcid.org/0000-0002-9297-5133>
 Ryan Gamurot  <https://orcid.org/0000-0001-5991-0808>
 Tateki Goto  <https://orcid.org/0000-0002-9540-6112>
 Bruno Guillet  <https://orcid.org/0000-0003-4091-0247>
 Jean-Marie Laugier  <https://orcid.org/0000-0002-1908-6057>
 Pablo Lewin  <https://orcid.org/0000-0003-0828-6368>

Margaret A. Loose  <https://orcid.org/0000-0002-5215-4779>
 Benjamin Mirwald  <https://orcid.org/0000-0002-1368-8815>
 Bruce Parker  <https://orcid.org/0000-0002-9578-5765>
 Michael Primm  <https://orcid.org/0000-0003-3462-7533>
 Justus Randolph  <https://orcid.org/0000-0001-6733-5380>
 Jay Runge  <https://orcid.org/0000-0003-4524-3340>
 Chelsea E. Sharon  <https://orcid.org/0000-0002-6250-5608>
 Jenny Shih  <https://orcid.org/0000-0002-6106-349X>
 Masao Shimizu  <https://orcid.org/0000-0002-3764-0138>
 Georges Simard  <https://orcid.org/0000-0002-9619-2996>
 Kevin Wagner  <https://orcid.org/0000-0002-4309-6343>
 Stefan Will  <https://orcid.org/0000-0003-0404-6279>

References

- Akeson, R. L., Chen, X., Ciardi, D., et al. 2013, *PASP*, **125**, 989
- Astropy Collaboration, Price-Whelan, A. M., Sipőcz, B. M., et al. 2018, *AJ*, **156**, 123
- Astropy Collaboration, Robitaille, T. P., Tollerud, E. J., et al. 2013, *A&A*, **558**, A33
- Beatty, T. G., & Gaudi, B. S. 2008, *ApJ*, **686**, 1302
- Benz, W., Broeg, C., Fortier, A., et al. 2020, *ExA*, **51**, 109
- Borucki, W. J., Koch, D., Basri, G., et al. 2010, *Sci*, **327**, 977
- Bradley, L., Sipocz, B., Robitaille, T., et al. 2022, astropy/photutils v1.4.0, Zenodo, doi:10.5281/zenodo.4044744
- Bryant, E. M., Bayliss, D., Santerne, A., et al. 2021, *MNRAS*, **504**, L45
- Cazeneuve, D., Marchis, F., Blaclard, G., et al. 2022, arXiv:2210.16440
- Chachan, Y., Dalba, P. A., Knutson, H. A., et al. 2022, *ApJ*, **926**, 62
- Cubillos, P., Harrington, J., Lored, T. J., et al. 2017, *AJ*, **153**, 3
- Dalba, P. A., Kane, S. R., Dragomir, D., et al. 2022, *AJ*, **163**, 61
- Dalba, P. A., Kane, S. R., Li, Z., et al. 2021, *AJ*, **162**, 154
- Dalba, P. A., & Tamburo, P. 2019, *ApJ*, **873**, L17
- Dragomir, D., Harris, M., Pepper, J., et al. 2020, *AJ*, **159**, 219
- Foreman-Mackey, D., Morton, T. D., Hogg, D. W., Agol, E., & Schölkopf, B. 2016, *ApJ*, **152**, 206
- Fossey, S. J., Waldmann, I. P., & Kipping, D. M. 2009, *MNRAS*, **396**, L16
- Gaia Collaboration, Prusti, T., de Bruijne, J. H. J., et al. 2016, *A&A*, **595**, A1
- Gaia Collaboration, Vallenari, A., Brown, A. G. A., et al. 2022, arXiv:2208.00211
- Garcia-Melendo, E., & McCullough, P. R. 2009, *ApJ*, **698**, 558
- Herman, M. K., Zhu, W., & Wu, Y. 2019, *ApJ*, **157**, 248
- Higson, E., Handley, W., Hobson, M., & Lasenby, A. 2018, *Stat. Comput.*, **29**, 891
- Kane, S. R. 2007, *MNRAS*, **380**, 1488
- Kane, S. R., Mahadevan, S., von Braun, K., Laughlin, G., & Ciardi, D. R. 2009, *PASP*, **121**, 1386
- Kipping, D. M., Torres, G., Henze, C., et al. 2016, *ApJ*, **820**, 112
- Lambert, R. A., Marchis, F., Asencio, J., et al. 2022, *Proc. SPIE*, **12182**, 121822Z
- Lang, D., Hogg, D. W., Mierle, K., Blanton, M., & Roweis, S. 2010, *ApJ*, **139**, 1782
- Laughlin, G., Deming, D., Langton, J., et al. 2009, *Natur*, **457**, 562
- Marchis, F., Arbouch, E., Bertin, E., et al. 2019, *EPSC*, **13**, 898
- Marchis, F., Malvache, A., Marfisi, L., Borot, A., & Arbouch, E. 2020, *AcAau*, **166**, 23
- Maxted, P. F. L., Ehrenreich, D., Wilson, T. G., et al. 2022, *MNRAS*, **514**, 77
- Maxted, P. F. L., & Gill, S. 2019, *A&A*, **622**, A33
- NASA Exoplanet Archive 2022, Planetary Systems Table, Version: 2022-09-02, NExSci-Caltech/IPAC, doi:10.26133/NEA12
- Pearson, K. A., Beichman, C., Fulton, B. J., et al. 2022, *AJ*, **164**, 178
- Ricker, G. R., Winn, J. N., Vanderspek, R., et al. 2014, *JATIS*, **1**, 014003
- Speagle, J. S. 2020, *MNRAS*, **493**, 3132
- Tsiganis, K., Gomes, R., Morbidelli, A., & Levison, H. F. 2005, *Natur*, **435**, 459
- Uehara, S., Kawahara, H., Masuda, K., Yamada, S., & Aizawa, M. 2016, *ApJ*, **822**, 2
- Von Braun, K., Kane, S. R., & Ciardi, D. R. 2009, *ApJ*, **702**, 779
- Walsh, K. J., Morbidelli, A., Raymond, S. N., O'Brien, D. P., & Mandell, A. M. 2011, *Natur*, **475**, 206
- Wang, J., Fischer, D. A., Barclay, T., et al. 2015, *ApJ*, **815**, 127
- Wang, X.-Y., Rice, M., Wang, S., et al. 2022, *ApJL*, **926**, L8
- Werner, M. W., Roellig, T. L., Low, F. J., et al. 2004, *ApJS*, **154**, 1
- Zellem, R. T., Pearson, K. A., Blaser, E., et al. 2020, *PASP*, **132**, 054401